Proc. Natl. Acad. Sci. USA
Vol. 89, pp. 9681–9685, October 1992
Biophysics

Conformational substates in azurin

(protein dynamics/flash photolysis/azurin–NO recombination after photodissociation)

DAVID EHRENSTEIN AND G. ULRICH NIENHAUS*

Department of Physics, University of Illinois at Urbana-Champaign, 1110 West Green Street, Urbana, IL 61801

Communicated by Hans Frauenfelder, July 23, 1992 (received for review May 26, 1992)

ABSTRACT **Azurin is a small blue copper protein in the electron transfer chain of denitrifying bacteria. It forms a photolabile complex with nitric oxide (NO) at low temperatures. We studied the temperature dependence of the ligand binding equilibrium and the kinetics of the association reaction after photodissociation over a wide range of temperature (80–280 K) and time (10^{-6}–10^{2} s). The nonexponential rebinding below 200 K is independent of the NO concentration and is interpreted as internal recombination. The rebinding can be modeled with the Arrhenius law by using a single preexponential factor of 6.3 × 10^{8} s^{-1} and a Gaussian distribution of enthalpy barriers centered at 23 kJ/mol with a width of 11 kJ/mol. Above 200 K, a slower, exponential rebinding process appears. The dependence of the kinetics on the NO concentration characterizes this reaction as bimolecular rebinding. The binding kinetics of NO to azurin show impressive analogies to the binding of carbon monoxide to myoglobin. We conclude that conformational substates occur not only in heme proteins but also in proteins with different active sites and secondary structures.**

Experiments measuring the binding of small ligands to heme proteins have contributed considerably to our understanding of the relation between the structure, dynamics, and function of proteins (1, 2). Sperm whale myoglobin (Mb) has served as a model system in these studies. Mb, a small, globular protein of 17.8 kDa, consists of 153 amino acids folded into a globular structure with eight α-helices. Diatomic ligands (O_2, CO) bind at the heme iron. The rebinding after photodissociation is nonexponential in time at low temperatures. An important concept results from the kinetic studies—namely, that proteins do not exist in a unique, well-defined structure, but in a large number of slightly different structures, the conformational substates (CS). Evidence for CS also comes from analysis of the Debye–Waller factor in protein crystals by x-ray diffraction (3, 4) and from the inhomogeneity of spectral lines (5, 6). The CS appear to be grouped into different tiers with distinctly different free energy barriers between the substates, leading to a hierarchical model of the conformational energy landscape in MbCO (7, 8).

We believe that these concepts apply not only to MbCO but to proteins in general. Strong covalent bonds establish the primary sequence, while only relatively weak forces like hydrogen bonds and hydrophobic effects determine the folding into the three-dimensional structure. Consequently, the positions of the amino acids are not unique, and competition among neighboring amino acids for the energetically optimal configuration arises from the dense packing. These two effects, disorder and frustration, lead to a complex conformational energy landscape with many local minima, the CS. The hierarchical arrangement of the CS may reflect the hierarchy of structural features in proteins.

To study the generality of these concepts, we chose azurin (Az) (from *Pseudomonas aeruginosa*), a protein of similar size as Mb but with a different secondary structure and active site structure. Az is a small blue copper protein that serves as an electron carrier in certain bacterial redox chains. It has a molecular mass of 14 kDa and consists of 128 amino acid residues. The three-dimensional structure of Az can be described as an eight-stranded β-sandwich with a small α-helical "flap" of ≈20 residues on the outside (9–11). The copper ion is bound in the interior of the protein in a distorted trigonal–bipyramidal coordination geometry. Extensive studies of the physical and chemical properties of the copper site have been carried out (12). The copper center that gives rise to the intense blue color of the protein has been characterized by optical (13), electron paramagnetic resonance (EPR) (14–16), NMR (17), and Raman spectroscopy (18). Blue copper centers (type 1 copper) bind nitric oxide (NO) (19). On binding, the strong absorption band in Az at 628 nm is bleached. The Az–NO complex can easily be photodissociated, and the absorption band at 628 nm that is responsible for the blue color reappears.

Here we investigate the temperature dependence of the ligand binding equilibrium and the binding kinetics after photodissociation with spectroscopic experiments over a wide range of temperature and time. We find characteristic analogies between rate processes in Mb and Az.

MATERIALS AND METHODS

Lyophilized Az from *P. aeruginosa* was purchased from Sigma and used without further purification. The protein was dissolved in a mixture of 70% (vol/vol) glycerol/30% 0.1 M acetate buffer, pH 5.5, to obtain a protein concentration of ≈100 μM. While stirring the sample for an hour, the atmosphere above the solution was replaced several times by N_2 gas. Then the N_2 was replaced by NO gas (pressure, 1 bar; 1 bar = 100 kPa), and the solution was allowed to incubate for another hour. The sample was transferred anaerobically into a sealed cuvette and cooled to cryogenic temperatures.

Optical spectra were measured with an Olis-Cary 14 spectrometer, interfaced to an IBM PC/AT, with a resolution of 2 nm. A closed-cycle helium refrigerator (Helix Technology, CTI-CRYOGENICS, Waltham, MA) cooled the sample. The temperature of the sample was measured with a calibrated silicon diode sensor and was adjusted with a digital controller (model DRC93C; Lake Shore Cryotronics, Westerville, OH) in the range between 10 and 300 K. The rebinding kinetics were studied with a flash photolysis system that employs a 6-ns (full width at half maximum) pulse from a frequency-doubled, Q-switched Nd-YAG (yttrium/aluminum garnet) laser (532 nm; 300 mJ) for photolysis (model NY-61; Continuum, Santa Clara, CA). Rebinding was monitored with light from a tungsten lamp that passed through a monochro-

The publication costs of this article were defrayed in part by page charge payment. This article must therefore be hereby marked "*advertisement*" in accordance with 18 U.S.C. §1734 solely to indicate this fact.

Abbreviations: CS, conformational substates; Az, azurin; EPR, electron paramagnetic resonance.

*To whom reprint requests should be addressed.

mator set at 628 nm. The monitor beam intensity was kept low and yielded a photolysis rate coefficient of $<10^{-2}$ s^{-1}. The light intensity was measured with a photomultiplier tube (model R 928; Hamamatsu, Middlesex, NJ) and digitized with our homemade logarithmic time-base digitizer (Wondertoy II) (20) from 1 μs to 100 s. The sample was kept in a storage cryostat (model 10-DT; Janis Research, Wilmington, MA) equipped with a digital temperature controller.

EXPERIMENTAL RESULTS AND DISCUSSION

Equilibrium Properties. When NO is added to an Az solution at room temperature, only minimal absorption changes occur. As the temperature is lowered, the strong Cys(σS) → Cu($d_{x^2-y^2}$) charge transfer band at 628 nm continuously decreases and practically disappears at 200 K (Fig. 1). The decrease of the 628-nm band is accompanied by an increase of the absorbance on the blue side of the spectrum. An isosbestic point exists near 538 nm. After illumination of the sample below 200 K, the band at 628 nm reappears and subsequently decays again in the dark. These results have been explained by the formation of a photolabile Cu–NO complex (19). The temperature dependence of the equilibrium coefficient, $\Lambda(T)$, of the reaction

$$\text{Az} + \text{NO} \rightleftharpoons \text{AzNO} \qquad [1]$$

indicates that the NO ligand is rather weakly bound to the protein. To analyze the energetics of the reaction, we measured the absorption spectra of AzNO between 200 and 300 K. From the area of the 628-nm band, we determined the ratio of the concentrations [AzNO]/[Az]. The area has been corrected for an intrinsic temperature dependence of this band (21). We evaluated the change in free energy ΔG, enthalpy ΔH, and entropy ΔS (for a standard state of 0.1 MPa NO pressure above the sample) from the equilibrium coefficient by the equation

$$\Lambda(T) = \frac{[\text{AzNO}]}{[\text{Az}]} = \exp\left(-\frac{\Delta G}{RT}\right) = \exp\left(-\frac{\Delta H}{RT}\right)\exp\left(\frac{\Delta S}{R}\right). \qquad [2]$$

R is the universal gas constant and T is the absolute temperature. The van't Hoff plot, $\Lambda(T)$ versus $(10^3/T)$, in Fig. 2 is linear, in agreement with Eq. 2, and yields $\Delta H = -(46 \pm 5)$ kJ/mol and $\Delta S/R = -(24 \pm 3)$. In heme proteins, the bond between the ligand and the metal ion is much stronger. For example, the binding enthalpy of CO to Mb is $\Delta H = -90$ kJ/mol (1, 22).

Kinetic Experiments. Fig. 3 shows the kinetics of NO binding to Az after photodissociation. The absorbance change (ΔA) is taken to be proportional to the fraction of proteins, $N(t)$, that has not yet bound a ligand after time t.

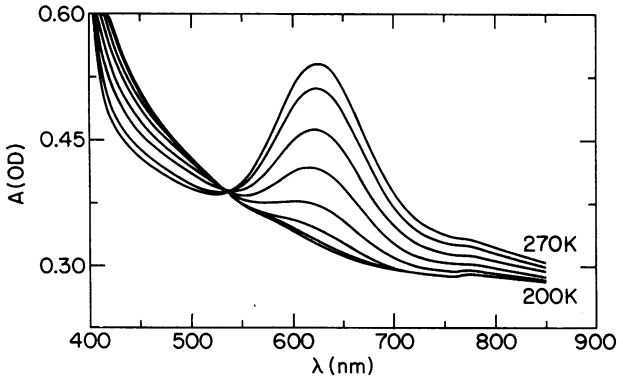

FIG. 1. Temperature dependence of AzNO absorbance spectra between 200 and 270 K.

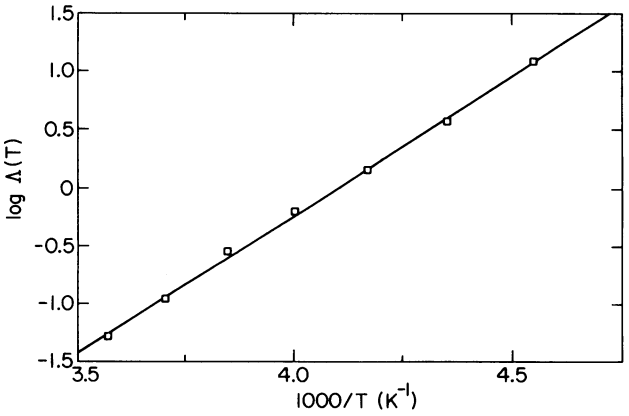

FIG. 2. van't Hoff plot of the equilibrium coefficient $\Lambda(T)$ = [AzNO]/[Az] for the binding of NO to Az.

Below 200 K, we observe nonexponential kinetics. At higher temperatures, a second process appears that is close to exponential in time. The kinetics of this reaction look sur-

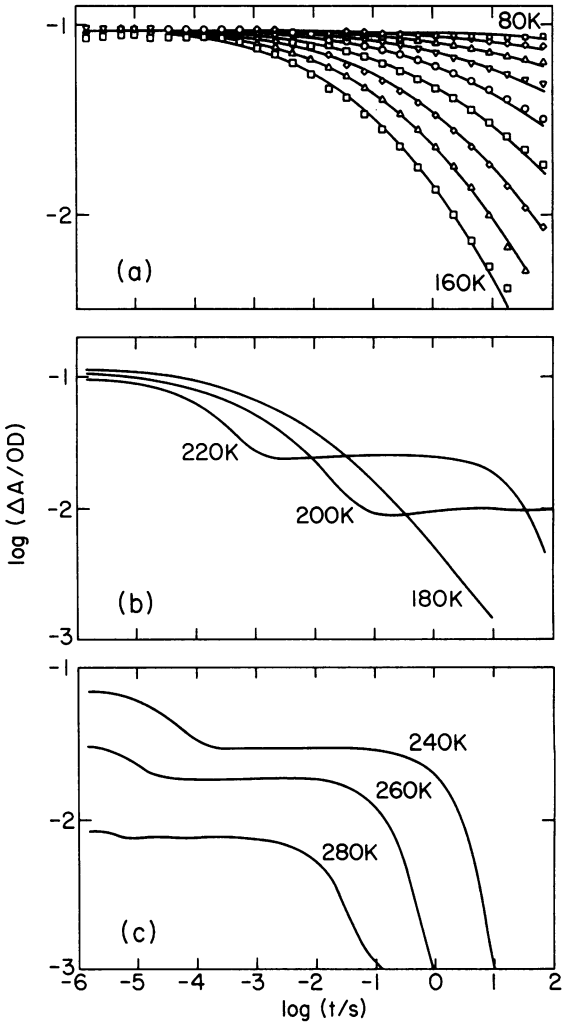

FIG. 3. Flash photolysis kinetics of AzNO at temperatures between 80 and 280 K. (*a*) Open symbols, experimental data between 80 and 160 K; solid lines, rebinding curves obtained from fitting a Gaussian enthalpy distribution $g(H_{BA})$ to the data. (*b*) Rebinding between 180 and 220 K. (*c*) Rebinding between 240 and 280 K. Above 200 K, the total signal decreases with increasing temperature because of the temperature dependence of the equilibrium coefficient $\Lambda(T)$. While the solvent process is insignificant below 180 K, it dominates the kinetics at the higher temperatures.

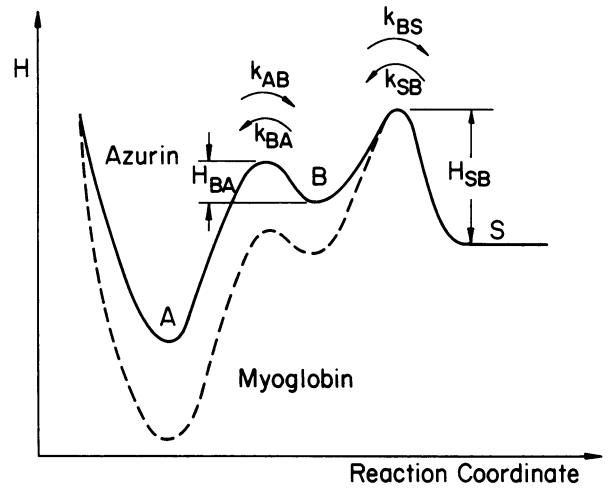

FIG. 4. Three-well model. Enthalpy barriers are plotted as a function of the reaction coordinate for AzNO (solid line) and MbCO (dashed line). Data for MbCO are taken from refs. 1 and 2.

prisingly similar to the kinetics of ligand binding to heme proteins and protoheme (1, 2, 23, 24). To describe the appearance of two temporally separated ligand association processes, a kinetic scheme with at least three distinct kinetic states is necessary. In heme proteins, the observed binding processes have been explained with the model depicted in Fig. 4, which shows the enthalpy of the system protein + ligand as a function of a reaction coordinate. It contains three wells (A, B, and S) in a reaction enthalpy surface. In well A, the ligand is bound to the metal ion. In well B, the ligand is in the vicinity of the reactive site and has to surmount an enthalpy barrier, H_{BA}, to bind. In well S, the ligand is in the solvent and has to overcome two sequential barriers, H_{SB} and H_{BA}, to bind. The kinetics are governed by the four rate coefficients k_{BA}, k_{AB}, k_{BS}, and k_{SB}, where k_{SB} is a pseudo-first-order rate coefficient in the presence of excess ligand. At temperatures below ≈200 K, the ligand cannot escape from the protein after photodissociation ($k_{BS} = 0$) and rebinds internally (process I; B → A). At higher temperatures, the ligand either rebinds internally or escapes to the solvent. Subsequently, a ligand from the solvent binds to the protein (process S; S → B → A).

The nonexponential kinetics at temperatures below ≈160 K (Fig. 3*a*) is a phenomenon that is familiar to us from studies of heme proteins in this temperature range (1, 2, 25, 26). In heme proteins, the nonexponential behavior has been explained with the concept of CS: At low temperatures, the proteins are frozen into many slightly different structures, the CS, with different activation enthalpies, H_{BA}, for ligand binding. The inhomogeneous ensemble of protein molecules is characterized by a distribution of enthalpy barriers, $g(H_{BA})$.† If we assume that $k_{AB} << k_{BA}$, the fraction of proteins that have not yet rebound a ligand at time t after photodissociation is described by

$$N(t, T) = \int g(H_{BA}) e^{-k_{BA}(H_{BA},T)t} dH_{BA}. \quad [3]$$

The temperature dependence of the rate coefficient $k_{BA}(H_{BA}, T)$ is usually given by the transition-state expression (26)

$$k_{BA}(H_{BA}, T) = A_{BA}(T/T_0) e^{-H_{BA}/RT}. \quad [4]$$

†In general, there will also be a distribution of activation entropies. Except for cases in which the enthalpy barriers are very low (e.g., protoheme-CO), the influence of the distributed activation entropy on the kinetics is negligible.

Here A_{BA} is the frequency factor, and T_0 is a reference temperature of 100 K. At very low temperatures, quantum-mechanical tunneling contributions to the rate coefficient $k(H_{BA}, T)$ may become important (27). We use Eqs. 3 and 4 to perform a nonlinear least-squares fit to the experimental data. The kinetics at the various temperatures are fitted simultaneously with a single, temperature-independent $g(H_{BA})$. We tried different model functions for $g(H_{BA})$ (28), but the Gaussian clearly gave the best fit. The solid lines in Fig. 3*a* show the fitted kinetic curves. The Gaussian enthalpy distribution $g(H_{BA})$ for binding of NO to Az has a maximum at 23 kJ/mol and a full width at half maximum of 11 kJ/mol. The preexponential A_{BA} is 6.3×10^8 s^{-1}.

In Fig. 5, we plot $g(H_{BA})$ for the low-temperature rebinding of AzNO and MbCO as determined by flash photolysis experiments with monitoring in the visible range. In Mb, the enthalpy distribution is narrower and peaked at much lower enthalpy values around 10 kJ/mol. It is asymmetric and can be described with a Γ distribution (29). The asymmetry arises mainly from the fact that Mb has three major substates, denoted A_0, A_1, and A_3 (8). They have different preexponentials and enthalpy distributions, which have been determined by flash photolysis with monitoring in the infrared (30). When measuring in the visible spectrum, all three A substates contribute. We have recently shown that the low-temperature rebinding kinetics of MbCO can be modeled with a sum of Gaussian distributions of the three A substates (28). Furthermore, temperature-derivative spectroscopy in the infrared at low temperatures also yields Gaussian enthalpy distributions for the individual A substates (31). Several theories attempt to explain the shapes of the $g(H_{BA})$ distributions. In these models, a protein coordinate, which represents the conformational inhomogeneity, is coupled to the reaction coordinate. Depending on the assumptions about the shape of the conformational distribution and the nature of the coupling, one arrives at either a symmetric (Gaussian) (32, 33) or an asymmetric $g(H_{BA})$ distribution (29, 34). Our results with MbCO and AzNO suggest that these low-temperature enthalpy distributions may be intrinsically symmetric and Gaussian. It is also interesting that the preexponential factors, A_{BA}, for Az and Mb are identical.

We have recently reported a time- and temperature-dependent relaxation of the structure in heme proteins after dissociation of the ligand. The relaxation occurs at temperatures >160 K and leads to an increase of H_{BA} (2, 35). In MbCO, the kinetics were explained by assuming that the barrier distribution, which is peaked around 10 kJ/mol below 160 K, shifts to about 22 kJ/mol during rebinding. To determine whether such a relaxation effect is present in AzNO, we compared the kinetics between 160 and 200 K with the prediction from the low-enthalpy distribution, which was

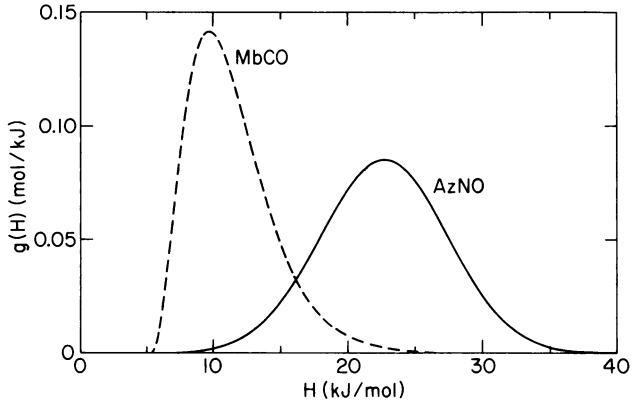

FIG. 5. Enthalpy distribution $g(H_{BA})$ from the low-temperature data of AzNO (see Fig. 3*a*) and MbCO (2).

obtained from the kinetics between 80 and 160 K. We found good agreement, indicating that no significant barrier relaxation process occurs after photodissociation of AzNO. In Mb and Hb, the conformational relaxation decreases the steric repulsion between the proximal histidine and the heme group. Evolution may have tailored this effect to optimize the functional properties of these proteins. In contrast, the Az structure shows a tight cluster of hydrogen bonds around the active site that prevents a structural transition. The rather rigid peptide environment may be important for the function of Az: to perform a fast electron transfer, the reduction or oxidation of the copper ion should not be accompanied by significant nuclear rearrangements.

Above 200 K, the fraction of ligands that escape to the solvent increases with temperature (Fig. 3). Concomitantly, the total amount of photolyzed molecules decreases because the equilibrium shifts toward the dissociated state. The binding of NO from the solvent is close to exponential for all temperatures. This behavior indicates that we are observing a pseudo-first-order reaction (excess ligand concentration) and that the ligands see an average binding enthalpy rather than a distribution when returning from the solvent. Protein fluctuations are responsible for this averaging effect (1, 2).

We have analyzed our kinetic data in the frame of the three-well model in the temperature range between 200 and 300 K. The general solution of the rate equations for the three-well model is straightforward but leads to rather clumsy expressions. In heme proteins, the analysis is simplified substantially by the fact that $k_{SB} << k_{BA}$, k_{BS}, and $k_{AB} = 0$ (2, 23). In this limit, the binding kinetics are given by

$$N(t) = N_I e^{-\lambda_I t} + N_S e^{-\lambda_S t}, \quad [5]$$

where λ_I and λ_S denote the apparent rate coefficients for the internal process and for the solvent process, respectively. In Az, the condition $k_{SB} << k_{BA}$, k_{BS} still holds, as indicated by the clear temporal separation (3–4 decades) of the solvent process from the internal process. The equilibrium experiments show weak binding of NO at higher temperatures. Therefore, k_{AB} cannot be neglected. The equilibrium coefficient is given by

$$\Lambda(T) = \frac{k_{SB}k_{BA}}{(k_{BS} + k_{SB})k_{AB}} \approx \frac{k_{SB}k_{BA}}{k_{BS}k_{AB}}. \quad [6]$$

Eq. 6 shows that $\Lambda(T) < 1$ does not imply that k_{AB} is comparable with k_{BA} but merely that the ratio k_{BA}/k_{AB} is less than the ratio k_{BS}/k_{SB}. In fact, we have $k_{AB} << k_{BA}$, k_{BS} in the studied temperature range and obtain for the apparent rate coefficients

$$\lambda_I = k_{BA} + k_{BS}, \qquad \lambda_S = \frac{k_{AB}k_{BS}}{k_{BA} + k_{BS}} + \frac{k_{BA}k_{SB}}{k_{BA} + k_{BS}}. \quad [7]$$

In the expression for λ_S, the first and the second terms represent the ligand dissociation and association, respectively. In heme systems, the dissociation can be neglected, and only the second term occurs in the expression for λ_S (2, 23).

We extract the four rate coefficients k_{BA}, k_{AB}, k_{BS}, and k_{SB} in the following way: at temperatures below ≈220 K, the majority of the molecules rebind internally, thus $k_{BA} >> k_{BS}$. In this limit, the association rate coefficient dominates, and $\lambda_S \approx k_{SB}$. At temperatures around 280 K, the majority of the molecules rebind from the solvent (process S; S → B → S), thus $k_{BS} >> k_{BA}$. Then the dissociation rate coefficient dominates, and $\lambda_S \approx k_{AB}$. Furthermore, the rate coefficient k_{BA} above 200 K can be calculated by averaging over the low-temperature barrier distribution $g(H_{BA})$ (see equations 33–36 in ref. 2). The extraction of k_{BS} is more complicated. Within the dynamic three-well model of Steinbach *et al.* (2), the internal rebinding ceases as protein fluctuations become fast compared to the characteristic time of the measurement for two reasons: (*i*) fluctuations average and effectively decrease the internal barrier, and (*ii*) fluctuations allow ligand escape from the protein. Therefore, we subtract the solvent process from our rebinding curves and take the inverse time of the drop-off of process I as an estimate for the rate coefficient k_{BS} for escape of the ligand into the solvent. The rate coefficients are plotted in Fig. 6.

The reaction enthalpy landscapes for AzNO and MbCO in Fig. 4 reflect the enthalpies determined from both the kinetics and the equilibrium studies. The enthalpy barrier H_{SB} that a ligand surmounts upon entering the protein is identical for the two systems. In MbCO, the enthalpy of state B is a few kJ/mol below state S, which indicates weak binding of the ligand in the heme pocket. In contrast to MbCO, the state B in Az is significantly higher than state S. This result makes sense because Az does not have a pocket, and the protein matrix may have to loosen up in order to accommodate the ligand. Finally, the well A is much deeper in Mb because of the stronger Fe-CO bond.

Within our analysis, the temperature dependence of λ_S (Fig. 6) implies that k_{AB} and k_{SB} are very similar. There is only a very slight curvature, indicating that k_{AB} has a larger activation enthalpy than k_{SB}. Consequently, we conclude from Eq. 6 that the equilibrium coefficient, $\Lambda(T)$, changes with temperature mainly because of the steeper temperature dependence of k_{BS} compared with k_{BA}, indicating that H_{BS} is larger than H_{BA}. The physical mechanisms that determine the two rate coefficients k_{AB} and k_{SB} are entirely different, and, therefore, there is no reason why they should be so similar. This behavior either is accidental or points to limitations of the three-well model. In Fig. 6, we also plot log λ_S for protoheme-CO (25). Both systems show a surprisingly similar temperature dependence of the solvent rebinding, which may indicate that λ_S is governed by the mobility of the ligand in the solvent and protein. For protoheme-CO, this effect has been discussed repeatedly in the literature (23, 24, 36). Assuming similar activities and diffusivities of NO and CO, the difference of ≈2 decades between the AzNO and protoheme-CO binding would then suggest that the entropic barrier for NO binding to Az is considerably larger, indicating that the binding site is less accessible in Az than in protoheme.

The AzNO Binding Reaction. Evidently, NO forms a photolabile complex with Az. Two scenarios appear reasonable: either a group on the protein surface binds the NO and transfers an electron to the copper or the NO binds directly to the Cu^{2+} ion, which is buried inside the protein with a minimum distance of 7.5 Å to the protein surface. Gorren *et*

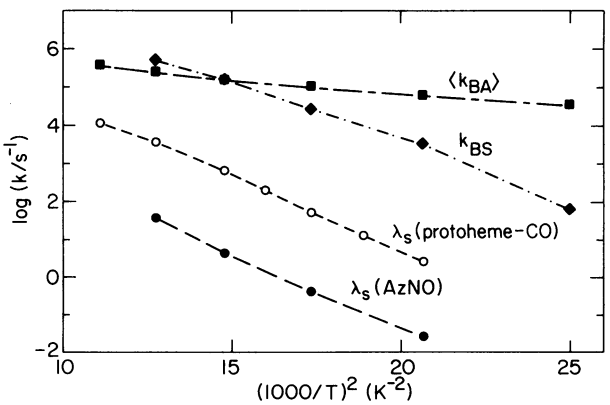

FIG. 6. Logarithmic plot of rate coefficients of AzNO versus $(1000/T)^2$ for temperatures between 200 and 300 K. For details of the analysis, see text. We also plot λ_S for protoheme-CO from ref. 23.

al. (19) discuss various models on the basis of their optical and EPR experiments at 77 K. It is interesting that the optical spectra change drastically, but the EPR signal, which disappears on NO binding, does not reappear after illumination of the sample at 77 K. To explain the EPR result, one has to assume that the NO is still close to the copper after photodissociation and hence not bound at the surface. Gorren *et al.* (19) favor the binding of NO in a diamagnetic charge transfer complex Cu^{+}–NO^{+}. We note that the binding of NO to Az is accompanied by the appearance of an absorption band below 400 nm. Such a band has been reported at 330 nm for the blue copper center in ascorbate oxidase on NO binding (37). It has been shown that the Cys(σS) → Cu($d_{x^2-y^2}$) charge transfer transition, which absorbs around 600–630 nm in blue copper centers, is located in the region around 350 nm in several tetragonal Cu^{2+} model complexes (13, 38). Therefore, one may speculate that the NO ligand is bound to the Az in a tetragonal Cu^{2+}–NO complex. Additional experiments, in particular x-ray structure analysis, will be necessary to clarify the binding geometry.

CONCLUSIONS

The binding of AzNO after photodissociation shows characteristic analogies to the effects observed in heme proteins. The geminate rebinding is nonexponential. Therefore, β-sheet proteins exhibit the same kinetic heterogeneity as α-helical proteins. The molecules exist in a large number of conformational substates with slightly different structures and functional properties. The fact that the Az molecule provides a rather rigid polypeptide environment that forces the copper ion into its functionally important coordination geometry does not preclude structural heterogeneity. Our results agree with EPR studies of Brill and collaborators (14–16) and with fluorescence experiments (39). The EPR spectrum at cryogenic temperatures was explained with a Gaussian distribution of the tetrahedral angle of the lobes of the ground state orbital of the cupric site. This result is in close agreement with our observation of a continuous distribution of enthalpy barriers. The fluorescence results were modeled by three discrete lifetimes, which have been associated with three conformational states. This interpretation, however, is not unambiguous. Because of its very narrow time window, a fluorescence experiment cannot distinguish between a small number of discrete states and a continuous distribution (40).

Above 200 K, we observe exponential binding of the ligands from the solvent. Therefore, the molecules fluctuate among the different conformational substates. The temperature dependence of the rate coefficient λ_S in AzNO is very similar to that obtained for protoheme-CO, which draws attention to the role of ligand diffusion in the binding reaction. While the reaction of Az and NO may not have any physiological relevance, it appears to be a useful tool for study of the conformational energy landscape in a β-sheet protein.

We thank B. Banko, K. Chu, D. C. Lamb, J. R. Mourant, J. Müller, R. Philipp, A. Xie, and R. D. Young for their collaboration. Special thanks are due to Prof. H. Frauenfelder for his continuous support and helpful criticism. This work was supported in part by the National Science Foundation (Grant DMB87-16476), the National Institutes of Health (Grant GM 18051), and the Office of Naval Research (Grant N00014-89-J-1300).

1. Austin, R. H., Beeson, K. W., Eisenstein, L., Frauenfelder, H. & Gunsalus, I. C. (1975) *Biochemistry* **14**, 5355–5373.
2. Steinbach, P. J., Ansari, A., Berendzen, J., Braunstein, D., Chu, K., Cowen, B. R., Ehrenstein, D., Frauenfelder, H., Johnson, J. B., Lamb, D. C., Luck, S., Mourant, J. R., Nienhaus, G. U., Ormos, P., Philipp, R., Xie, A. & Young, R. D. (1991) *Biochemistry* **30**, 3988–4001.
3. Frauenfelder, H., Petsko, G. A. & Tsernoglou, D. (1978) *Nature (London)* **280**, 558–563.
4. Hartmann, H., Parak, F., Steigemann, W., Petsko, G. A., Ringe Ponzi, D. & Frauenfelder, H. (1982) *Proc. Natl. Acad. Sci. USA* **79**, 4967–4971.
5. Campbell, B. F., Chance, M. R. & Friedman, J. M. (1987) *Science* **238**, 373–376.
6. Ormos, P., Ansari, A., Braunstein, D., Cowen, B. R., Frauenfelder, H., Hong, M. K., Iben, I. E. T., Sauke, T. B., Steinbach, P. J. & Young, R. D. (1990) *Biophys. J.* **57**, 191–199.
7. Ansari, A., Berendzen, J., Bowne, S. F., Frauenfelder, H., Iben, I. E. T., Sauke, T. B., Shyamsunder, E. & Young, R. D. (1985) *Proc. Natl. Acad. Sci. USA* **82**, 5000–5004.
8. Ansari, A., Berendzen, J., Braunstein, D., Cowen, B. R., Frauenfelder, H., Hong, M. K., Iben, I. E. T., Johnson, J. B., Ormos, P., Sauke, T. B., Scholl, R., Schulte, A., Steinbach, P. J., Vittitow, J. & Young, R. D. (1987) *Biophys. Chem.* **26**, 337–355.
9. Adman, E. T., Stenkamp, R. E., Sieker, L. C. & Jensen, L. H. (1978) *J. Mol. Biol.* **123**, 35–47.
10. Norris, G. E., Anderson, B. F. & Baker, E. N. (1983) *J. Mol. Biol.* **165**, 501–521.
11. Nar, H., Messerschmidt, A., Huber, R., van de Kamp, M. & Canters, G. W. (1991) *J. Mol. Biol.* **221**, 765–772.
12. Adman, E. T. (1985) in *Topics in Molecular and Structural Biology, Metalloproteins*, ed. Harrison, P. M. (Verlag Chemie, Weinheim, F.R.G.), Vol. 6, pp. 1–42.
13. Gray, H. B. & Solomon, E. I. (1981) in *Copper Proteins*, ed. Spiro, T. (Wiley, New York), pp. 1–39.
14. Brill, A. S. (1978) *Biophys. J.* **22**, 139–142.
15. Brill, A. S. (1979) in *Tunneling in Biological Systems*, eds. Chance, B. & DeVault, D. C. (Academic, New York), pp. 561–568.
16. Aqualino, A., Brill, A. S., Bryce, G. F. & Gerstman, B. S. (1991) *Phys. Rev. A* **44**, 5257–5271.
17. Ulrich, E. L. & Markley, J. C. (1978) *Coord. Chem. Rev.* **27**, 109–140.
18. Thamann, T. J., Frank, P., Willis, L. J. & Loehr, T. M. (1982) *Proc. Natl. Acad. Sci. USA* **79**, 6396–6400.
19. Gorren, A. C. F., de Boer, E. & Wever, R. (1987) *Biochim. Biophys. Acta* **916**, 38–47.
20. Berendzen, J., Frauenfelder, H., Sauke, T. & Scholl, R. (1989) *Bull. Am. Phys. Soc.* **34**, 880a (abstr.).
21. Cupane, A., Leone, M., Vitrano, E. & Cordone, L. (1990) *Biophys. Chem.* **38**, 213–224.
22. Keyes, M. H., Falley, M. & Lumry, R. (1970) *J. Am. Chem. Soc.* **93**, 2035–2040.
23. Alberding, N., Austin, R. H., Chan, S. S., Eisenstein, L., Frauenfelder, H., Gunsalus, I. C. & Nordlund, T. M. (1976) *J. Chem. Phys.* **65**, 4701–4711.
24. Miers, J. B., Postlewaite, J. C., Zyung, T., Chen, S., Roemig, G. R., Wen, X. & Dlott, D. D. (1990) *J. Chem. Phys.* **93**, 8771–8776.
25. Alberding, N., Chan, S. S., Eisenstein, L., Frauenfelder, H., Good, D., Gunsalus, I. C., Nordlund, T. M., Perutz, M. F., Reynolds, A. H. & Sorensen, L. B. (1978) *Biochemistry* **17**, 43–51.
26. Dlott, D. D., Frauenfelder, H., Langer, P., Roder, H. & DiIorio, E. E. (1983) *Proc. Natl. Acad. Sci. USA* **80**, 6239–6243.
27. Alben, J. O., Beece, D., Bowne, S. F., Eisenstein, L., Frauenfelder, H., Good, D., Marden, M. C., Moh, P. P., Reinisch, L., Reynolds, A. H. & Yue, K. T. (1980) *Phys. Rev. Lett.* **44**, 1157–1160.
28. Steinbach, P. J., Chu, K., Frauenfelder, H., Johnson, J. B., Lamb, D. C., Nienhaus, G. U., Sauke, T. B. & Young, R. D. (1992) *Biophys. J.* **61**, 235–245.
29. Young, R. D. & Browne, S. F. (1984) *J. Chem. Phys.* **81**, 3730–3737.
30. Young, R. D., Frauenfelder, H., Johnson, J. B., Lamb, D. C., Nienhaus, G. U., Philipp, R. & Scholl, R. (1991) *Chem. Phys.* **158**, 315–327.
31. Berendzen, J. & Braunstein, D. (1990) *Proc. Natl. Acad. Sci. USA* **87**, 1–5.
32. Agmon, N. & Hopfield, J. J. (1983) *J. Chem. Phys.* **79**, 2042–2053.
33. Stein, D. L. (1985) *Proc. Natl. Acad. Sci. USA* **82**, 3670–3672.
34. Srajer, V., Reinisch, L. & Champion, P. M. (1988) *J. Am. Chem. Soc.* **110**, 6656–6669.
35. Nienhaus, G. U., Mourant, J. R. & Frauenfelder, H. (1992) *Proc. Natl. Acad. Sci. USA* **89**, 2902–2906.
36. Caldin, E. F. & Hasinoff, B. B. (1975) *J. Chem. Soc. Faraday Trans.* **71**, 515–527.
37. van Leeuwen, F. X. R., Wever, R., van Gelder, B. F., Avigliano, L. & Mondovi, B. (1975) *Biochim. Biophys. Acta* **403**, 285–291.
38. Amundsen, A. R., Whelan, J. & Bosnich, B. (1977) *J. Am. Chem. Soc.* **99**, 6730–6739.
39. Hutnik, C. M. & Szabo, A. G. (1989) *Biochemistry* **28**, 3923–3934.
40. Alcala, J. R., Gratton, E. & Prendergast, F. G. (1987) *Biophys. J.* **51**, 587–596.